

# The Remarkable Afterglow of GRB 061007: Implications for Optical Flashes and GRB Fireballs

C. G. Mundell<sup>1</sup>, A. Melandri<sup>1</sup>, C. Guidorzi<sup>1,2,3</sup>, S. Kobayashi<sup>1</sup>, I. A. Steele<sup>1</sup>, D. Malesani<sup>4</sup>, L. Amati<sup>5</sup>, P. D'Avanzo<sup>3,6</sup>, D. F. Bersier<sup>1</sup>, A. Gomboc<sup>1,7</sup>, E. Rol<sup>8</sup>, M. F. Bode<sup>1</sup>, D. Carter<sup>1</sup>, C. J. Mottram<sup>1</sup>, A. Monfardini<sup>1,9</sup>, R. J. Smith<sup>1</sup>, S. Malhotra<sup>10</sup>, J. Wang<sup>11</sup>, N. Bannister<sup>8</sup>, P. T. O'Brien<sup>8</sup>, N. R. Tanvir<sup>8</sup>.

(cgm)@astro.livjm.ac.uk

## ABSTRACT

We present a multiwavelength analysis of *Swift* GRB 061007. The 2-m robotic Faulkes Telescope South (FTS) began observing 137 s after the onset of the  $\gamma$ -ray emission, when the optical counterpart was already decaying from  $R \sim 10.3$  mag, and continued observing for the next 5.5 hours. These observations begin during the final  $\gamma$ -ray flare and continue through and beyond a long, soft tail of  $\gamma$ -ray emission whose flux shows an underlying simple power-law decay identical to that seen at optical and X-ray wavelengths, with temporal slope  $\alpha \sim 1.7$  ( $F \propto t^{-\alpha}$ ). This remarkably simple decay in *all* of these bands is rare for *Swift* bursts, which

---

<sup>1</sup>Astrophysics Research Institute, Liverpool John Moores University, Twelve Quays House, Birkenhead, CH41 1LD, UK

<sup>2</sup>Dipartimento di Fisica, Università di Milano-Bicocca, Piazza delle Scienze 3, 20126 Milano, Italy

<sup>3</sup>INAF-Osservatorio Astronomico di Brera, via Bianchi 46, 23807 Merate (LC), Italy

<sup>4</sup>International School for Advanced Studies (SISSA-ISAS), via Beirut 2-4, I-34014 Trieste, Italy

<sup>5</sup>INAF - IASF Bologna, via P. Gobetti 101, Bologna, Italy

<sup>6</sup>Università dell'Insubria, Dipartimento di Fisica e Matematica, via Valleggio 11, I-22100 Como, Italy

<sup>7</sup>FMF, University in Ljubljana, Jadranska 19, 1000 Ljubljana, Slovenia.

<sup>8</sup>Department of Physics and Astronomy, University of Leicester, University Road, Leicester LE1 7RH, UK

<sup>9</sup>CNRS-CTBT, 25 Avenue des Martyrs, 38000 Grenoble, France

<sup>10</sup>School of Earth and Space Exploration, Arizona State University, P.O. Box 871404, Tempe, AZ 85287-1404

<sup>11</sup>Center for Astrophysics, University of Science and Technology of China, Hefei, Anhui 230026, P. R. China

often show much more complex light curves. We suggest the afterglow emission begins as early as 30 – 100 s and is contemporaneous with the on-going variable prompt emission from the central engine, but originates from a physically distinct region dominated by the forward shock. The afterglow continues unabated until at least  $\sim 10^5$  seconds showing no evidence of a break. The observed multiwavelength evolution of GRB 061007 is explained by an expanding fireball whose optical, X-ray and late-time  $\gamma$ -ray emission is dominated by emission from a forward shock with typical synchrotron frequency,  $\nu_m$ , that is already below the optical band as early as  $t=137$  s and a cooling frequency,  $\nu_c$ , above the X-ray band to at least  $t=10^5$  s. In contrast, the typical frequency of the reverse shock lies in the radio band at early time. We suggest that the unexpected lack of bright optical flashes from the majority of *Swift* GRBs may be explained with a low  $\nu_m$  originating from small microphysics parameters,  $\epsilon_e$  and  $\epsilon_B$ . We derive a minimum jet opening angle  $\theta = 4.7^\circ$  from the optical light curves and conclude that GRB 061007 is a secure outlier to spectral energy correlations because no X-ray jet break occurred before  $t \sim 10^6$  s.

*Subject headings:* gamma rays: bursts – shock waves – radiation mechanisms: nonthermal – cosmology: observations

## 1. Introduction

Gamma-ray bursts (GRBs) are the most instantaneously luminous cosmological objects known, and although their transient nature makes them observationally challenging to follow up at other wavelengths after the initial burst of  $\gamma$  rays, their brightness and large redshift range ( $0.0085 < z < 6.29$ ) ensure they remain uniquely useful as probes of the early Universe. With the launch of the GRB-dedicated *Swift* satellite (Gehrels et al. 2004), early-time monitoring of the radiation from GRBs across the electromagnetic spectrum is now possible. Rapid and accurate localisation of GRBs and immediate dissemination of their positions drive ground-based follow-up campaigns with small and large optical and infrared robotic telescopes such as ROTSE, REM, the Liverpool and Faulkes Telescopes, while *Swift*'s on-board narrow field instruments the X-Ray Telescope (XRT) and the UltraViolet Optical Telescope (UVOT) observe a large fraction of GRBs within minutes of their detection with the Burst Alert Telescope (BAT).

Following the detection of a very bright optical counterpart to GRB 990123 by ROTSE (Akerlof et al. 1999) contemporaneous with the  $\gamma$ -ray emission and consistent with models predicting optical emission from a reverse shock in the relativistic outflow (Sari & Piran 1999;

Kobayashi & Sari 2000; Kobayashi 2000; Nakar & Piran 2005), there was strong anticipation of routine detection of optical flashes at early times with UVOT, which can detect optical emission below the detection threshold of ROTSE. However, despite rapid and accurate localisation of  $\gamma$ -ray emission and subsequent follow-up by UVOT, bright optical flashes remain elusive (Roming et al. 2006). In some cases, the high redshift of the burst renders it undetectable due to the lack of UVOT filters redder than V-band (i.e.  $z > 4$ ); in others, intrinsic faintness coupled with local extinction pushes the OT below the detection threshold of the UVOT (Oates et al. 2006). Ground-based observations from large robotic telescopes, optimised for the rapid follow-up of GRB alerts (Guidorzi et al. 2005; Guidorzi et al. 2006a; Dai et al. 2006), are increasing the number of well-sampled, early-time multicolor optical light curves over a wide range of magnitudes (Gomboc et al. 2006; Melandri et al. 2006) and revealing more complex decays than expected from pre-Swift light curves (Guidorzi et al. 2005; Stanek et al. 2006; Dai et al. 2006; Monfardini et al. 2006; Oates et al. 2006). Small departures from a power-law decay (i.e.  $\Delta m \lesssim 0.5$  mag) are interpreted as interactions between the expanding fireball and dense clumps in the circumburst medium (Lazzati et al. 2002; Heyl & Perna 2003; Nakar et al. 2003; Guidorzi et al. 2005) while major rebrightenings suggest late-time energy injections (Kumar & Piran 2000; Sari & Mészáros 2000; Zhang & Mészáros 2002; Stanek et al. 2006; Wozniak et al. 2006; Monfardini et al. 2006); bright optical flares consistent with reverse shocks, however, are still rare or unconfirmed (Boër et al. 2006; Jelínek et al. 2006). Complex light curves are now common at X-ray energies with *Swift* light curves revealing a canonical shape comprising a “3-segment” structure inconsistent with a single power-law decay, with X-ray flares superimposed in at least 50% of bursts. Such complexity has been a major surprise of the *Swift* era and has led to a general acceptance of long-lived activity (Burrows et al. 2005; O’Brien et al. 2006), challenging standard central engine models. A significant minority of GRB X-ray light curves show a fairly smooth decay consistent with an afterglow at early time (O’Brien et al. 2006) but most of these cases lack simultaneous optical data sufficient to fully test current models.

Here we present multicolor BVR*i*’ light curves of the very bright optical counterpart to GRB 061007 obtained automatically by the 2-m robotic telescope, the Faulkes Telescope South (FTS) at Siding Spring, Australia which began observing 137 s after the onset of the  $\gamma$ -ray emission when the optical counterpart was already decaying from  $R \sim 10.3$  mag, and continued observing for the next 5.5 hours<sup>1</sup>. We show that GRB 061007 is unusual for a *Swift* burst in that it shows a remarkably simple power-law decay from  $\gamma$  rays to optical wavelengths. Its isotropic equivalent radiated energy is one of the highest ever measured ( $E_{\text{iso}} \sim 10^{54}$  erg) and its peak  $\nu F_{\nu}$  energy,  $E_{\text{peak}}$ , is well-determined. It therefore provides a useful test

---

<sup>1</sup>Observations obtained as part of the RoboNet-1.0 project: <http://www.astro.livjm.ac.uk/RoboNet/>

of current spectral energy correlations without the complication of highly-structured light curves (Amati et al. 2002; Ghirlanda et al. 2004; Liang & Zhang 2005; Firmani et al. 2006; Amati 2006).

The multiwavelength observations and analyses are presented in Section 2; results and discussion are presented in Section 3, where a shock model is proposed to explain the observed multiwavelength evolution and broad-band spectral energy distribution. We end by considering implications for cosmological spectral energy correlations and present our conclusions in Section 4. Throughout,  $1\text{-}\sigma$  errors are given unless otherwise stated.

## 2. Observations and Analysis

On 2006 Oct 07, 10:08:08 UT<sup>2</sup> *Swift*-BAT detected GRB 061007 (trigger 232683) at coordinates R.A.(J2000)=03:05:16, Dec(J2000)=−50:29:15 (3 arc-min 90% containment radius). The prompt emission from GRB 061007 was also detected at MeV energies by *Konus/Wind* (20 keV–10 MeV) (Golenetskii et al. 2006), *Suzaku/WAM* (50 keV–5 MeV) (Yamaoka et al. 2006) and *RHESSI* (20 keV–10 MeV) (Wigger et al. 2006), whose detections provide estimates of the peak energy  $E_{\text{peak}}$  of  $399_{-18}^{+19}$  keV (Golenetskii et al. 2006),  $561_{-27}^{+29}$  keV (Yamaoka et al. 2006) and  $391_{-52}^{+58}$  keV (Wigger et al. 2006) respectively. The *Swift*-BAT  $\gamma$ -ray light curve shows three significant flat-topped peaks with substantial sub-structure, and a small fourth peak (from  $t_0+75$ s) that shows long exponential decay and faint emission detectable to  $t \sim 900$  s (Markwardt et al. 2006; Schady et al. 2006c). The fluence,  $S_\gamma = 2.49 \times 10^{-4}$  erg  $\text{cm}^{-2}$ , measured by *Konus-Wind*, corresponds to an isotropic equivalent energy  $E_{\text{iso}} \sim 10^{54}$  erg (Golenetskii et al. 2006) for the spectroscopic redshift  $z = 1.261$  (Osip et al. 2006; Jakobsson et al. 2006). The *Swift* XRT and UVOT began observing 80 s after the BAT trigger time and identified a very bright X-ray/optical counterpart with a rapid decay rate  $\alpha_x = 1.6 \pm 0.1$  ( $F \propto t^{-\alpha}$ ) (Schady et al. 2006a; Vetere et al. 2006; Schady et al. 2006b).

Robotically-triggered photometric observations with ground-based telescopes ROTSE and the FTS began at 26 and 137 s respectively, each identifying the optical counterpart with brightnesses 13.6 mag (unfiltered) (Rykoff et al. 2006) and 10.3 mag (R-band) (Mundell et al. 2006; Bersier et al. 2006) respectively at R.A.(J2000)=03:05:19.56, Dec(J2000)=−50:30:2.6 ( $\pm 1''2$ ). After taking the initial  $3 \times 10$  s exposure R-band images, the FTS continued to observe for the next 5.5 hours, cycling through  $BRi'$  filters with V imaging interspersed and using increasing exposure times, until finishing with a 300-s V-band image at UT=15:39:25.322. Initial photometric calibration was performed with GAIA (Optimal PSF Photometry Tool)

---

<sup>2</sup> $t=0$  throughout the paper.

relative to all the catalogued stars (USNO B1 and NOMAD) in the  $4'6 \times 4'6$  field of view and the bright star near the OT (RA=03:05:23.5, Dec=-50:30:16.6) was used for PSF determination. A  $5 \times 120$  s R-band image was also acquired using FORS1 on the VLT at 2006 Oct 8.04702 UT (0.6247 days after the burst); the observing conditions were photometric and calibration was performed relative to Landolt standard stars. The FTS R-band were adjusted to the VLT photometry to provide a well-calibrated R-band light curve. Later-time R-band images were acquired with the IMACS instrument on the Magellan-I Baade telescope at Las Campanas Observatory on Oct 9 and 10 and calibrated with respect to the VLT image. Finally, magnitudes are corrected for Galactic extinction: from  $E_{B-V} = 0.020$  (Schlegel et al. 1998), and  $A_V = R_V \cdot E_{B-V} = 0.06$  mag, with  $R_V = 3.1$ , we evaluated the extinction in the other filters following Cardelli et al. (1989):  $A_B = 0.08$  mag,  $A_R = 0.05$  mag and  $A_V = 0.04$  mag. Fluxes were derived following Fukugita et al. (1996) and calibration uncertainties for the remaining FTS filters, which do not affect the overall light curve properties, were taken into account when deriving the broad-band spectral energy distribution. Results are summarized in Table 1 and plotted in Figure 1 along with the mask-tagged background subtracted BAT light curve, which was produced by the standard BAT pipeline (HEADAS v 6.1.1). The BAT light curve was masked with the ground-refined coordinates provided by the BAT team (Markwardt et al. 2006). BAT spectra have been corrected for systematics with the “*batphasyserr*” tool and the original 80 energy channels have been grouped to have  $3\text{-}\sigma$  significant grouped channels. We processed XRT data from 200 s to 400 s after the trigger adopting standard screening and we extracted the XRT 0.3–10 keV spectrum: data were in Window Timing (WT) mode and the average count rate was below 100 counts  $\text{s}^{-1}$  so that no correction for pileup was required (Romano et al. 2006).

The brightness of the burst and the similarity of the decay rate in all bands (see Figure 1 and Table 2) allows the construction of an early-time broad-band spectral energy distribution (SED), shown in Figure 2. The joint XRT/BAT 0.3–150 keV spectrum from 200 s to 400 s is well fit with a power law with significant absorption in excess of the Galactic,  $N_{\text{H}}(\text{Gal}) = 1.75 \times 10^{20} \text{ cm}^{-2}$  (Kalberla et al. 2005), such that  $\beta_{\text{X-}\gamma} = 1.01 \pm 0.03$  ( $F \propto \nu^{-\beta}$ ) and rest-frame  $N_{\text{H}} = (5.8 \pm 0.4) \times 10^{21} \text{ cm}^{-2}$  (90% confidence level). As shown in Figure 2 and Table 3, when  $\beta$  is free to vary, the best fit is obtained for  $\beta_{\text{opt-X-}\gamma} = 1.02 \pm 0.05$  and  $A_V = 0.48 \pm 0.19$  mag with an SMC-like extinction profile (Pei 1992).

### 3. Results and Discussion

Figure 1 shows the FTS BVR*i'* and background-subtracted *Swift*-BAT light curves of GRB 061007; a single power-law decay with  $\alpha = 1.72 \pm 0.10$  ( $F \propto t^{-\alpha}$ ) provides a good

fit to all optical light curves for  $t < 40$  min, resulting in small residuals in this time range and emphasizing the presence of an additional broad, multicolor bump over the time range  $40 < t < 350$  min (see Table 2). Late-time VLT R-band photometry confirms that the underlying power-law decay continues, showing no evidence for a break before 1000 min (0.624 d). This is consistent with the continuation of the simple power-law decay in the XRT light curve (Schady et al. 2006c). Similarly, the marginal Magellan detection extends the continuation of the unbroken power-law decay to  $t = 2495$  min (1.73 d), and, combined with the final upper limit  $R > 23.3$  mag at 4087 min (2.84 d - Table 1), constrains the brightness of the host galaxy. A similar power law ( $\alpha = 1.7 \pm 0.1$ ) also provides a good fit to the decay of the long, soft tail of the  $\gamma$ -ray emission for  $t > 120$  s, although slight modulation of the power law due to the intrinsic variability is evident, as illustrated in the expanded view of the light curves of the first 10 min (Figure 1 right panel; Table 2). A similar deviation from the R-band power law may be present at  $\sim 2.3$  min (see residuals Figure 1), coincident in time with a small  $\gamma$ -ray flare, but the effect is marginal.

The broad-band spectral energy distribution shown in Figure 2 confirms the overall common power-law decay in all bands from  $\gamma$  to optical and is well fitted by an absorbed power law with optical extinction  $A_V \sim 0.48 \pm 0.19$  mag with an SMC profile. Comparing this with the  $N_H$  derived from the X-ray spectrum, we find a deficit of optical extinction, as already found in most GRBs (Stratta et al. 2004; Kann et al. 2006; Galama & Wijers 2001). In principle this could be explained in a number of ways (see e.g. the case of GRB 051111, Guidorzi et al. 2006b): 1) an extinction profile different from those typical of MW, SMC, LMC (e.g. Stratta et al. 2004; Savaglio & Fall 2004); 2) a population of dust grains skewed towards big sizes, possibly as a result of dust destruction due to the GRB itself (e.g. Maiolino et al. 2001; Chen et al. 2006); 3) a significant presence of molecular gas (1999); 4) overabundance of some alpha metals responsible for absorption in X-rays (e.g., GRB 050401, Watson et al. 2006).

Below, we explain the observed multiwavelength evolution of GRB 061007 at  $t > 70$  s with an expanding fireball whose optical, X-ray and  $\gamma$ -ray emission is dominated by synchrotron emission from a forward shock whose cooling frequency lies above the X-ray band and typical synchrotron frequency lies just below the optical band; in contrast, the typical frequency of the reverse shock lies in the radio band at early time, with the typical frequency of the forward shock entering the radio band at  $\sim 2.5$  days after the burst.

### 3.1. Forward Shock Emission from a Decelerating Fireball

The optical and X-ray afterglow light curves are described by the same power law  $\alpha \sim 1.7$  to more than  $10^5$  sec after the burst; this indicates that these photons are radiated from the same forward shock, and optical and X-ray bands are in the same domain of a synchrotron spectrum<sup>3</sup>. In principle a bump of a forward shock (blast wave) light curve, as seen for  $t > 40$  min (Figure 1), can be produced by inhomogeneity of the ambient medium or by energy injection into a blast wave. However, energy injection causes a transition from a blast wave to another with a larger energy, and it leads to a shift of the afterglow decay baseline after the bump (at this late time the evolution of a blast wave is adiabatic). Since the optical flux comes back to the pre-bump decay line, inhomogeneity of ambient medium is favored to explain the bump around 100 min in the optical. The X-ray band (and the optical band) should be below the synchrotron cooling frequency  $\nu_c$ , otherwise the inhomogeneity in the ambient medium does not produce an afterglow bump (Kumar 2000). For the synchrotron shock model, the decay index and spectral index at frequencies  $\nu_m < \nu < \nu_c$  are  $\alpha = 3(p - 1)/4$  and  $\beta = (p - 1)/2$ , respectively (Sari, Piran and Narayan 1998). With  $p \sim 3$  these give reasonable fits to the observed indices. We note that if a burst occurred in a wind medium with density  $n \propto R^{-s}$ , the decay index in this spectral domain  $\nu_m < \nu < \nu_c$  is given by  $\alpha = [2s + 3(p - 1)(4 - s)]/(16 - 4s) \sim 1.7$  for  $p = 3$  and  $s = 1$  (Monfardini et al. 2006). The additional parameter  $s$  allows a better fits to the decay index, but still a rather large value of  $p \sim 3$  is required to explain the observed  $\beta$ .

Since the optical and X-ray light curves show no break during the observations, the typical synchrotron frequency  $\nu_m \propto t^{-3/2}$  should be already below the optical band  $\nu_m < \nu_{opt} \sim 5 \times 10^{14}$  Hz before our earliest optical observation was made at  $t = 137$  sec, while the cooling frequency  $\nu_c \propto t^{-1/2}$  should be still above X-ray band  $\nu_X < \nu_c \sim 10^{18}$  Hz at  $t \sim 10^5$  sec. Using the results in Sari, Piran and Narayan (1998), we get

$$\nu_m(t) \sim 1.0 \times 10^{21} \zeta^{1/2} \epsilon_B^{1/2} \epsilon_e^2 E_{54}^{1/2} t_m^{-3/2} \text{ Hz}, \quad (1)$$

$$\nu_c(t) \sim 6.8 \times 10^{12} \zeta^{-1/2} \epsilon_B^{-3/2} E_{54}^{-1/2} n^{-1} t_m^{-1/2} \text{ Hz} \quad (2)$$

where  $\zeta = (1 + z)/2.26$ ,  $E_{54} = E/10^{54}$  ergs,  $t_m$  is the observer's time in units of min,  $n$  is the density in  $\text{cm}^{-3}$ ,  $\nu_m$  is proportional to  $(p - 2)/(p - 1)$  and we have assumed  $p = 3$ . The requirements for the break frequencies at  $t = 137$  s and at  $t = 10^5$  s give constraints on the

---

<sup>3</sup>Even if we assume reverse shock emission, the observed bands should be in the same spectral domain  $\nu_m < \nu_{opt}, \nu_X < \nu_c$ , because reverse shock emission above the cooling frequency vanishes after the shock crossing. In this case we obtain the theoretical value  $\alpha - 3\beta/2 \sim 1$  which is not consistent with observation  $\alpha - 3\beta/2 \sim 0$

microphysics parameters,

$$\epsilon_B < 3.0 \times 10^{-5} n^{-2/3} (\zeta E_{54})^{-1/3} \quad (3)$$

$$\epsilon_e < 1.7 \times 10^{-2} \left( \frac{\epsilon_B}{3.0 \times 10^{-5}} \right)^{-1/4} (\zeta E_{54})^{-1/4} \quad (4)$$

These energy partition values are somewhat small but are not inconsistent with values derived for other bursts (e.g. Panaitescu & Kumar 2002).

### *Onset of the Afterglow and Lack of Optical Flash*

ROTSE detected a 13.6-mag optical counterpart at 26 s after the GRB trigger (Rykoff et al. 2006). This magnitude is dimmer than the extrapolation of our observations. It indicates that the afterglow peaked between 26 s and 137 s, and very likely around the end of the main pulses of the prompt emission  $t_p \sim 100$  s. Using this peak time, we can estimate the Lorentz factor of the fireball at that time (Sari and Piran 1999). It is

$$\Gamma \sim \left( \frac{3(1+z)^3 E}{32\pi n m_p c^5 t_p^3} \right)^{1/8} \sim 230 \left( \frac{t_p}{10^2 \text{sec}} \right)^{-3/8} (\zeta^3 E_{54}/n)^{-1/8} \quad (5)$$

It is interesting that the tail of the  $\gamma$ -ray emission is described by the same power-law decay  $\alpha \sim 1.7$  as the optical and X-ray emission (Figure 1); indeed the flux at the dip in the prompt phase at  $\sim 40$  s is consistent with the underlying power-law line. If the afterglow started at  $\sim 30$  s, the Lorentz factor is  $\sim 360$ . No jet break within  $10^5 \text{ s}^4$  gives a lower limit of the GRB jet opening angle  $\theta_0(\text{rad}) > 0.07 n^{1/8} E_{54}^{-1/8} \zeta^{-3/8} (t/10^5 \text{sec})^{3/8}$ .

There is no reverse shock emission component even though the optical observations started right after the prompt emission phase. We can explain the lack of optical flash naturally in the standard model if the typical frequency of the forward shock emission is lower than optical band  $\nu_m < \nu_{opt}$  at the onset of afterglow (the peak time  $t_p$ ). At the peak time (the shock crossing time), the forward and reverse shocked regions have the same Lorentz factor and internal energy density, the cooling frequency of the reverse shock is equal to that of the forward shock  $\nu_{c,r}(t_p) \sim \nu_c(t_p)$ . The matter density in the reverse shocked region is much higher than in the forward shock region, and it makes the electron

---

<sup>4</sup>Another possible scenario is that a jet break happened immediately after the prompt phase at  $t < 100$  sec. This scenario requires a very small electron index to explain the decay indices of the optical and X-ray light curves.



temperature lower. The typical frequency of the reverse shock is much lower than that of the forward shock  $\nu_{m,r}(t_p) \ll \nu_m(t_p) < \nu_{opt}$  (e.g. Kobayashi & Zhang 2003).

The shock regions have the same amount of shock energies at  $t_p$ , and their luminosities ( $\sim \nu F_\nu$  at  $\nu_c$ ) are comparable at  $t_p$ . Considering that the two emission components have the same spectral index, at  $t_p$  they contribute equally to the flux at any observed frequency between  $\nu_{m,f}$  and  $\nu_c$ . After the shock crossing  $t > t_p$  the reverse shock emission decays more rapidly as  $\sim t^{-2}$ , so the contribution from the reverse shock should be masked by the forward shock component in the decay phase.

Forward shock emission peaks when a fireball decelerates or when the typical frequency passes through the observed band. If an optical peak is not associated with a spectral change from  $\nu^{1/3}$  to  $\nu^{-(p-1)/2}$ , it could be because of the deceleration of a fireball, and the typical frequency could be located below the observed band at that time. In such a case, the optical flash should always be absent. In recent years, ground-based robotic telescopes reported the lack of optical flashes, except for a few cases. The lack might be explained with low  $\nu_m$  originating from rather small microphysics parameters,  $\epsilon_e$  and  $\epsilon_B$ . GRB 060117 and GRB 061007 might be clear example cases.

### 3.2. Implications for Late-Time Radio Emission

After the deceleration, the emission frequency of each electron in the shocked ejecta (reverse shock region) drops quickly with time as  $\nu_e \propto t^{-73/48}$ . Both the typical frequency and cooling frequency drop with this scaling, because after a reverse shock has crossed the ejecta (deceleration), no new electrons are injected and all electrons cool by adiabatic expansion only. The peak power decays as  $F_{\nu,max} \propto t^{-47/48}$ . The flux below or above the typical frequency  $\nu_{m,r}$  evolves as (Sari & Piran 1999; Kobayashi & Sari 2000, their Eq. 3),

$$F_\nu \propto \begin{cases} t^{-17/36} & \nu < \nu_{m,r}, \\ t^{-(73p+21)/96} \propto t^{-5/2} \quad (p = 3) & \nu > \nu_{m,r}. \end{cases} \quad (6)$$

The optical afterglow of GRB 061007 was very bright. If the forward shock typical frequency is close to the optical band at the deceleration time  $\nu_m(t_p) \sim 5 \times 10^{14}$  Hz, extrapolating our observational results to the deceleration time  $t_p \sim 100$  s, we obtain the peak flux of the forward shock emission  $F_{\nu,max} \sim 420$  mJy. The typical frequency of the reverse shock emission is lower by a factor of  $\sim \Gamma^2$  (Kobayashi & Zhang 2002), and it is in the radio band  $\nu_{m,r}(t_p) \sim \nu_m/\Gamma^2 \sim 9.5(\Gamma/230)^{-2}$  GHz. At the deceleration time, the peak flux of the reverse shock emission is larger by a factor of  $\Gamma \sim 230$  than that of the forward shock emission. Since the reverse shock emission in the radio band initially decays as  $t^{-17/36}$  until

the typical frequency passage, then as  $t^{-5/2}$ , the reverse shock radio emission at 1 day is about  $\sim 8.6 (\nu/4.8\text{GHz})^{-1}(t/1\text{day})^{-5/2}\mu\text{Jy}$ .

The typical frequency of the forward shock emission  $\nu_m \propto t^{-3/2}$  comes to radio band  $\nu = 4.8 \text{ GHz}$  about 2.5 day after the burst. Before the passage, the flux increases as  $t^{1/2}$ , and then decays as  $t^{-1.7}$ . The peak value is expected to be  $\sim 420 \text{ mJy}$ . At low frequencies and early times, self absorption plays an important role and significantly reduces the afterglow flux. A simple rough estimate of the maximum flux is the emission from a black body with the shock temperature (e.g. Sari & Piran 1999; Kobayashi & Sari 2000). The temperature is given by the random energy of the typical electron  $k_B T \sim m_e c^2 \gamma_m \sim \epsilon_e m_p c^2 \Gamma / 2$  for  $p=3$ . If the observed frequency is above the typical frequency, the electrons radiating into the observed frequency have an energy higher than the typical energy,  $m_e c^2 \gamma_m$ , by a factor of  $(\nu/\nu_m)^{1/2}$ . Following the notation of Sari & Piran (1999), the upper limit of blackbody emission is

$$F_\nu^{BB} = \pi(R_\perp/d)^2 \Gamma S_\nu \quad (7)$$

where  $d = d_L/(1+z)^{1/2}$  and  $S_\nu = (2\nu^2/c^2)k_B T$ . Therefore

$$F_\nu^{BB} \sim \pi(1+z)m_p\nu^2\epsilon_e\Gamma^2\left(\frac{R_\perp}{d_L}\right)^2, \quad (8)$$

$$\sim 6\left(\frac{\nu}{4.8\text{GHz}}\right)^2\left(\frac{t}{1\text{day}}\right)^{1/2}\epsilon_{e,-2}(E_{54}/n)^{1/2}\text{ mJy} \quad (9)$$

where  $\epsilon_{e,-2} = \epsilon_e/10^{-2}$  and  $R_\perp \sim 4.6\Gamma ct$  is the observed size of the fireball, assuming  $z = 1.26$  and  $d_L = 2.7 \times 10^{28} \text{ cm}$ . Note that other emission estimates use only scalings (normalizations are given by the observations), the blackbody upper limit is more model dependent.

The results from ATCA (van der Horst et al. 2006a,b) give even lower limits about  $50\mu\text{Jy}$  level. Their formal flux measurements are  $-25 \pm 45\mu \text{ Jy}$  (1.00-1.24 days after the burst) and  $-1 \pm 43\mu\text{Jy}$  (5.03-5.28 days after) at 4.8 GHz. Although the blackbody limit is possibly less reliable, the radio non-detection might imply a high-density environment  $n \gg 1$ . The peak flux of the forward shock emission is given by (Sari, Piran & Narayan 1998),

$$F_{\nu,max}(z = 1.26) \sim 20 \left(\frac{\epsilon_B}{5 \times 10^{-5}}\right)^{1/2} E_{54} n^{1/2} \text{ mJy} \quad (10)$$

As can be seen from Equations 3 and 10, the dependence of  $F_{\nu,max}$  on density is weak ( $\sim n^{1/6}$ ), and thus the bright afterglow cannot be easily explained by a high density environment.

### 3.3. GRB 061007 and Cosmological Spectral–Energy Correlations

*Swift* GRB 061007 is one of the most luminous GRBs ever detected and thus, with its high-quality  $\gamma$ -ray data, well-characterised light curves and well-determined peak energy, it is an ideal object to test the cosmological spectral–energy correlations, namely the  $E_{\text{peak}}-E_{\text{iso}}$  (Amati et al. 2002),  $E_{\text{peak}}-E_{\gamma}$  (Ghirlanda et al. 2004) and  $E_{\text{peak}}-E_{\text{iso}}-t_{\text{b}}$  (Liang & Zhang 2005) correlations. As described in Section 2 the prompt  $\gamma$ -ray emission at MeV energies was detected by three additional satellites which provide estimates of the peak energy. While the peak energies measured by *Konus/Wind* and *RHESSI* are comparable, that measured by *Suzaku/WAM* is significantly larger; in addition to possible systematics, this may be explained by the fact that this instrument measured the brightest part of the GRB, as suggested by their low duration estimate (T90 $\sim$ 50 s vs 90 s measured by *Konus/Wind*)<sup>5</sup>. We therefore use the spectral information from *Konus/Wind* and *RHESSI*, conservatively assuming an  $E_{\text{peak}}$  range including both 90% c.l. intervals provided by the two instruments, i.e.  $E_{\text{peak}}=394\pm 55$  keV, corresponding to a cosmological rest-frame peak energy of  $890\pm 124$  keV.

The isotropic–equivalent radiated energy is  $E_{\text{iso}}=(1.0\pm 0.1)\times 10^{54}$  erg in the 1-10000 keV cosmological rest–frame, assuming  $H_0 = 70$  km/s/Mpc,  $\Omega_{\Lambda} = 0.3$  and  $\Omega_m = 0.7$  and a Band spectral shape (Band et al. 1993) with parameters and fluence provided by *Konus/Wind* (Golenetskii et al. 2006). Following Amati (2006) the  $E_{\text{peak}}-E_{\text{iso}}$  correlation predicts a corresponding  $E_{\text{peak}} = 907$  keV, fully consistent with the measured value for GRB 061007. Thus, GRB 061007 further confirms the validity of the  $E_{\text{peak}}-E_{\text{iso}}$  correlation in the very high radiated energy regime and since this correlation should only hold for prompt emission, confirms that GRB 061007 has prompt emission typical of other *Swift* bursts on the correlation, despite its unusually simple afterglow emission.

Finally, the test of the  $E_{\text{peak}}-E_{\gamma}$  and  $E_{\text{peak}}-E_{\text{iso}}-t_{\text{b}}$  correlations, which is of particular importance given their possible use for the estimate of cosmological parameters (e.g. Firmani et al. 2005) requires the detection of a late break in the afterglow light curves. As can be seen in Figure 1, our optical light curves show no evidence of a break up to  $\sim 150$  ks and the XRT light curve continues unbroken to at least  $10^6$  s (Schady et al. 2006c), providing a firm lower limit to the jet break time. Combining our estimates of  $E_{\text{iso}}$  and the lower limit to the jet opening angle of  $\sim 4.7^\circ$  inferred from the optical light curve, we derive a collimation-corrected energy  $E_{\gamma} > 3.4\times 10^{51}$  erg; this limit would predict  $E_{\text{peak}} > 1274$  keV in order to be consistent with the  $E_{\text{peak}}-E_{\gamma}$  correlation (Nava et al. 2006), a value somewhat higher

---

<sup>5</sup>The lower bound of the energy band of WAM is somewhat higher than that of *Konus/Wind* and *RHESSI*, which may result in an overestimate of  $E_{\text{peak}}$  (Amati 2006).

than the measured value of  $890 \pm 124$  (90% c.l.). By accounting for the logarithmic dispersion of this correlation (Nava et al. 2006), the deviation of the measured value from this lower limit is  $\sim 1.6 \sigma$ . Better consistency is found with the  $E_{\text{peak}}-E_{\text{iso}}-t_b$  correlation, which, when adopting the parameters reported by Liang & Zhang (2005) predicts a lower limit to  $E_{\text{peak}}$  of 986 keV. Using the lower limit to the jet break time  $t \sim 10^6$  s suggested by the X-ray light curve, we conclude that GRB 061007 becomes a secure outlier to both  $E_{\text{peak}}-E_{\gamma}$  and  $E_{\text{peak}}-E_{\text{iso}}-t_b$  correlations, deviating by more than  $3 \sigma$ . X-ray light curves for other GRBs suggest the existence of a population of objects similar to GRB 061007 that are inconsistent with these correlations (Sato et al. 2006; Willingdale et al. in prep.), although optical observations were not available for these objects. GRB 061007 might therefore transpire to be the norm rather than an anomaly.

#### 4. Conclusions

We have presented a multiwavelength study of the very bright GRB 061007 based on optical observations that cover the period from 137 s to 3 days after the burst and *Swift* XRT and BAT data. We conclude that the afterglow commences as early as 30 – 100 s after the onset of the GRB and the optical, X-ray and underlying  $\gamma$ -ray emission, which are described by the same power-law decay  $\alpha \sim 1.7$  after this time, represent photons that are radiated from the same forward shock, with optical and X-ray bands in the same domain of a synchrotron spectrum. In contrast, the typical frequency of the reverse shock emission is already in the radio domain at early time, explaining the lack of a bright early-time optical flash and late time radio flare. We note the similarity of the light curves of GRB 061007 to that of GRB 060117, which was only observed in a single optical filter (Jelínek et al. 2006) and suggest it too may represent the onset of an early afterglow similar to GRB 061007. Finally, we highlight the simplicity of the early-onset afterglow of GRB 061007, which with its well-behaved light curves, typical circumburst environment and well-determined peak  $\gamma$ -ray energy, make it a useful candidate for inclusion in current cosmological correlations. We find that this event is fully consistent within  $1 \sigma$  with the  $E_{\text{peak}}-E_{\text{iso}}$  correlation and also potentially consistent within  $1.6 \sigma$  with the  $E_{\text{peak}}-E_{\gamma}$  and  $E_{\text{peak}}-E_{\text{iso}}-t_b$  correlations using a lower limit to the jet break time  $t_b$ , and thus to  $E_{\gamma}$ , derived from our data. We note that since the X-ray afterglow continued without a jet break until  $t > 10^6$  s, this event is firm outlier to the  $E_{\text{peak}}-E_{\gamma}$  and  $E_{\text{peak}}-E_{\text{iso}}-t_b$  correlations, deviating from these correlations by more than  $\sim 3 \sigma$ .

CGM acknowledges financial support from the Royal Society. AXM, MFB, ER, PTO, acknowledge funding from the Particle Physics and Astronomy Research Council (PPARC).

RoboNet1.0 and Swift are supported by PPARC. The Faulkes Telescopes, now owned by Las Cumbres Observatory, are operated with support from the Dill Faulkes Educational Trust. This work is partly based on data taken with ESO telescopes at VLT under program 078.D-0752. We thank the kind assistance of the observing staff at Paranal. We thank J.E. Rhoads for assistance in acquiring the Magellan data, L. Nava for input on the spectral correlations and the anonymous referee for useful comments and suggestions.

## REFERENCES

- Akerlof, C., et al. 1999, *Nature*, 398, 400
- Amati L. et al., 2002, *A&A*, 390, 81
- Amati, L. 2006, *MNRAS*, 372, 233
- Arabadjis, J.S., & Bregman, J.N. 1999 *ApJ*, 510, 806
- Band, D. et al. 1993 *ApJ*, 413, 281
- Bersier et al. 2006, *GCN Circ.* 5709
- Boër, M., Atteia, J.L., Damerджи, Y., Gendre, B., Klotz, A. & Stratta, G. 2006 *ApJ*, 623, L71
- Burrows, D. N. et al. 2006 Proceedings of the "The X-ray Universe 2005", 26-30 September 2005, El Escorial, Madrid, Spain. Organised by European Space Agency (ESA). Ed. by A. Wilson. ESA SP-604, Volume 2, Noordwijk: ESA Publications Division, 2006, p.877
- Cardelli, J. A., Clayton, G. C., & Mathis, J. S. 1989 *ApJ*, 345, 245
- Chen, S.L., Li, A.G., & Wei, D.M. 2006 *ApJ*, 647, L13
- Dai, X., Halpern, J.P., Morgan, N.D., Armstrong, E., Mirabal, N., Haislip, J.B., Reichart, D.E. & Stanek, K.Z. 2006, *astro-ph/0609269*
- Firmani C., Ghisellini G., Avila-Reese V., Ghirlanda G., 2006, *MNRAS*, 370, 185
- Fukugita, M., et al. 1996, *AJ*, 111 Number 4, 1748
- Galama, T.J. & Wijers, A.M.J. 2001 *ApJ*, 549, L209
- Gehrels, N., et al. 2004 *ApJ*, 611, 1005

- Ghirlanda G., Ghisellini G., Lazzati D. 2004, ApJ, 616, 331
- Golenetskii, S. et al. 2006, GCN Circ. 5722
- Gomboc et al. 2006, to appear in "Swift and GRBs:Unveiling the Relativistic Universe", II Nuovo Cimento, in press
- Guidorzi, C., et al. 2005 ApJ, 630 Issue 2, L121
- Guidorzi, C., et al. 2006, PASP, 118 N.840, 288
- Guidorzi, C. et al. 2006, A&A, submitted
- Heyl, J.S. & Perna, R. 2003 ApJ, 586, L13
- Jakobsson, P. et al. 2006, GCN Circ. 5716
- Jelínek, M. et al. 2006, A&A, 454, L119
- Kalberla, P.M.W., Burton, W.B., Hartmann, D., Amal, E.M., Bajaja, E., Morras, R., & Pöppel, W.G.L., 2005, A&A, 440, 775
- Kann, D.A., Klose, S. & Zeh, A. 2006 ApJ, 641, 993
- Kobayashi, S. & Sari, R. 2000 ApJ, 542, 819
- Kobayashi, S. 2000 ApJ, 545, 807
- Kobayashi, S. & Zhang, B. 2003 ApJ, 582, L75
- Kumar, P. 2000 ApJ, 538, L125
- Kumar, P. & Piran, T. 2000 ApJ, 532, 286
- Lazzati, D., Rossi, E., Covino, S., Ghisellini, G., & Malesani, D. 2002, A&A, 396, L5
- Liang E. & Zhang B., 2005, ApJ, 633, 611
- Maiolino, R., Marconi, A., & Oliva, E. 2001, A&A, 365, 37
- Markwardt, C. 2006, GCN Circ. 5713
- Melandri, A. et al. 2006, to appear in "The Multicolored Landscape of Compact Objects, AIP Conf. Proc, in preparation
- Monfardini, A. et al. 2006, ApJ, 648, 1125

- Mundell, C. et al. 2006, GCN Circ. 5708
- Nakar, E., Piran, T., Granot, J. 2003, *New Astronomy*, 8, 495
- Nakar, E. & Piran, T. 2005, *ApJ*, 619, L147
- Nava, L., Ghisellini, G., Ghirlanda, G., Tavecchio, F., & Firmani, C. 2006, *A&A*, 450, 471
- Oates, S., et al. 2006, *MNRAS*, 372, 327
- O'Brien, P. et al. 2006, *ApJ*, 647, 1213
- Osip, D. et al. 2006, GCN Circ. 5715
- Panaitescu, A. and Kumar, P. 2002 *ApJ*, 571, 779
- Pei, Y.C. 1992 *ApJ*, 395, 130
- Romano, P. et al., 2006, *A&A*, 456, 917
- Roming, P. et al., 2006 *ApJ*, in press (astro-ph/0509273)
- Rykoff et al. 2006, GCN Circ. 5706
- Sari, R. & Piran, T. 1999, *A&AS*, 138, 537
- Sari, R. & Mészáros, P. 2000 *ApJ*, 535,L33
- Sari, R., Piran, T. & Narayan,R. 1998 *ApJ*, 497, L17
- Sato, G. et al. 2006 *ApJ*, accepted
- Savaglio, S. & Fall, S.M. 2004 *ApJ*, 614, 293
- Schady et al. 2006a, GCN Circ. 5707
- Schady et al. 2006b, GCN Circ. 5719
- Schady et al. 2006c, *MNRAS*, submitted (astro-ph/0611081)
- Schlegel, D. J., Finkbeiner, D. P., & Davis, M. 1998 *ApJ*, 500, 525
- Stanek, K. Z., Dai, X. et al. 2006, astro-ph/0602495
- Stratta, G., Fiore, F., Antonelli, L.A., Piro, L. & de Pasquale, M. 2004 *ApJ*, 608, 846
- van der Horst, A.J., Rol, E. et al. 2006a, GCN Circ. 5720

van der Horst, A.J., Rol, E. et al. 2006b, GCN Circ. 5726

Vetere, L. et al. 2006, GCN Circ. 5712

Watson, D. et al. 2006, ApJ, in press (astro-ph/0510368)

Wigger, C. et al. 2006, GCN Circ. 5725

Wozniak, P. R., Vestrand, J.A., Wren, J.A., White, R.R., Evans, S.M., Casperson, D. 2006  
ApJ, 642, L99

Yamaoka, K. et al. 2006, GCN Circ. 5724

Zhang, B. & Mészáros, P. 2002 ApJ, 566, 712



Table 1. FTS, VLT and Magellan optical observations of GRB 061007.

TELESCOPE	$\Delta T$ (MIN)	FILTER	EXPOSURE TIME (s)	MAG $\pm$ ERR <sup>†</sup>
FTS	2.28	R <sub>C</sub>	10.0	10.34 $\pm$ 0.11
	2.63	R <sub>C</sub>	10.0	10.68 $\pm$ 0.12
	3.00	R <sub>C</sub>	10.0	10.96 $\pm$ 0.11
	4.63	B	10.0	12.81 $\pm$ 0.20
	5.52	V	10.0	12.52 $\pm$ 0.20
	6.38	SDSS- <i>i'</i>	10.0	11.67 $\pm$ 0.04
	7.50	B	30.0	13.56 $\pm$ 0.10
	8.80	R <sub>C</sub>	30.0	12.85 $\pm$ 0.10
	12.25	SDSS- <i>i'</i>	30.0	13.03 $\pm$ 0.04
	16.73	B	60.0	15.18 $\pm$ 0.09
	18.42	R <sub>C</sub>	60.0	14.28 $\pm$ 0.10
	20.18	SDSS- <i>i'</i>	60.0	13.90 $\pm$ 0.11
	21.93	B	120.0	15.64 $\pm$ 0.07
	24.63	R <sub>C</sub>	120.0	14.78 $\pm$ 0.08
	27.38	SDSS- <i>i'</i>	120.0	14.47 $\pm$ 0.10
	30.15	B	180.0	16.24 $\pm$ 0.09
	33.78	R <sub>C</sub>	180.0	15.36 $\pm$ 0.08
	37.55	SDSS- <i>i'</i>	180.0	15.04 $\pm$ 0.09
	41.45	B	120.0	16.70 $\pm$ 0.09
	44.08	R <sub>C</sub>	120.0	15.71 $\pm$ 0.08
	46.83	SDSS- <i>i'</i>	120.0	15.31 $\pm$ 0.10
	49.63	B	180.0	16.92 $\pm$ 0.10
	53.28	R <sub>C</sub>	180.0	15.98 $\pm$ 0.07
	57.07	SDSS- <i>i'</i>	180.0	15.59 $\pm$ 0.09
	60.85	B	240.0	17.27 $\pm$ 0.11
	68.40	R <sub>C</sub>	30.0	16.25 $\pm$ 0.09
	70.50	B	10.0	17.48 $\pm$ 0.11
	71.23	V	10.0	17.16 $\pm$ 0.21
72.13	SDSS- <i>i'</i>	10.0	15.94 $\pm$ 0.11	
73.17	B	30.0	17.66 $\pm$ 0.13	

Table 1—Continued

TELESCOPE	$\Delta T$ (MIN)	FILTER	EXPOSURE TIME (S)	MAG $\pm$ ERR <sup>†</sup>
	74.40	R <sub>C</sub>	30.0	16.48 $\pm$ 0.09
	75.62	SDSS- <i>i'</i>	30.0	16.06 $\pm$ 0.10
	76.90	B	60.0	17.66 $\pm$ 0.20
	78.53	R <sub>C</sub>	60.0	16.59 $\pm$ 0.09
	80.32	SDSS- <i>i'</i>	60.0	16.15 $\pm$ 0.10
	82.08	B	120.0	17.78 $\pm$ 0.18
	84.77	R <sub>C</sub>	120.0	16.72 $\pm$ 0.09
	87.52	SDSS- <i>i'</i>	120.0	16.30 $\pm$ 0.09
	90.30	B	180.0	17.92 $\pm$ 0.16
	93.95	R <sub>C</sub>	180.0	16.95 $\pm$ 0.09
	97.73	SDSS- <i>i'</i>	180.0	16.51 $\pm$ 0.10
	101.55	B	120.0	18.18 $\pm$ 0.17
	104.20	R <sub>C</sub>	120.0	17.03 $\pm$ 0.08
	106.93	SDSS- <i>i'</i>	120.0	16.63 $\pm$ 0.10
	109.68	B	180.0	18.36 $\pm$ 0.14
	113.43	R <sub>C</sub>	180.0	17.26 $\pm$ 0.08
	117.20	SDSS- <i>i'</i>	180.0	16.87 $\pm$ 0.11
	120.98	B	240.0	18.67 $\pm$ 0.17
	125.62	R <sub>C</sub>	240.0	17.50 $\pm$ 0.15
	145.55	R <sub>C</sub>	300.0	17.55 $\pm$ 0.11
	150.92	R <sub>C</sub>	300.0	17.65 $\pm$ 0.10
	160.12	V	450.0	18.38 $\pm$ 0.18
	171.98	B	450.0	19.25 $\pm$ 0.15
	191.77	SDSS- <i>i'</i>	300.0	17.57 $\pm$ 0.13
	197.15	SDSS- <i>i'</i>	300.0	17.63 $\pm$ 0.12
	203.75	R <sub>C</sub>	300.0	18.19 $\pm$ 0.11
	209.13	R <sub>C</sub>	150.0	18.20 $\pm$ 0.11
	215.67	V	600.0	18.90 $\pm$ 0.17
	242.75	B	300.0	19.62 $\pm$ 0.20
	249.33	SDSS- <i>i'</i>	300.0	18.17 $\pm$ 0.13

Table 1—Continued

TELESCOPE	$\Delta T$ (MIN)	FILTER	EXPOSURE TIME (S)	MAG $\pm$ ERR <sup>†</sup>
	254.72	SDSS- <i>i'</i>	300.0	18.17 $\pm$ 0.12
	261.28	R <sub>C</sub>	600.0	18.95 $\pm$ 0.13
	273.20	V	600.0	19.38 $\pm$ 0.20
	295.43	B	600.0	20.09 $\pm$ 0.26
	307.42	SDSS- <i>i'</i>	600.0	18.39 $\pm$ 0.15
	319.37	R <sub>C</sub>	300.0	19.20 $\pm$ 0.25
	331.28	V	300.0	19.99 $\pm$ 0.30
VLT	899.58	R <sub>C</sub>	600.0	21.48 $\pm$ 0.03
Magellan	2494.80	R <sub>C</sub>	240.0	23.65 $\pm$ 0.50
	4086.64	R <sub>C</sub>	240.0	>23.30

<sup>†</sup>Quoted errors for BV*i'* filters are statistical. Absolute calibration requires inclusion of the systematic error 0.25 mag due to the uncertainty in the USNO B1 photometric calibration. This error has been fully included when deriving the SED (See Figure 2 and Table 3).

Table 2: Results of power-law fits to optical and  $\gamma$ -ray light curves as shown in Figure 1.

Band	Time Range For Fit	Temporal Power-Law Decay ( $\alpha$ )
B	$t < 40$ min	$1.72 \pm 0.05$
V	–	Fixed to $\alpha_R$
R	$t < 40$ min	$1.72 \pm 0.01$
$i'$	$t < 40$ min	$1.75 \pm 0.06$
BAT(15 – 350 keV)	$t > 40$ s	$1.7 \pm 0.1$

Table 3: Best-fitting parameters derived from optical-X- $\gamma$  spectral energy distribution.

	SMC <sup>‡</sup>	LMC	MW	SMC, $\beta_{X\gamma}$ fixed
$\beta$	$1.02 \pm 0.05$	$1.03 \pm 0.05$	$1.03 \pm 0.05$	1.01
$A_V$ (mag)	$0.48 \pm 0.19$	$0.54 \pm 0.20$	$0.54 \pm 0.20$	$0.29 \pm 0.06$
$\chi^2/\text{d.o.f}$	195/174	195/174	195/174	197/175

<sup>‡</sup>See Figure 2

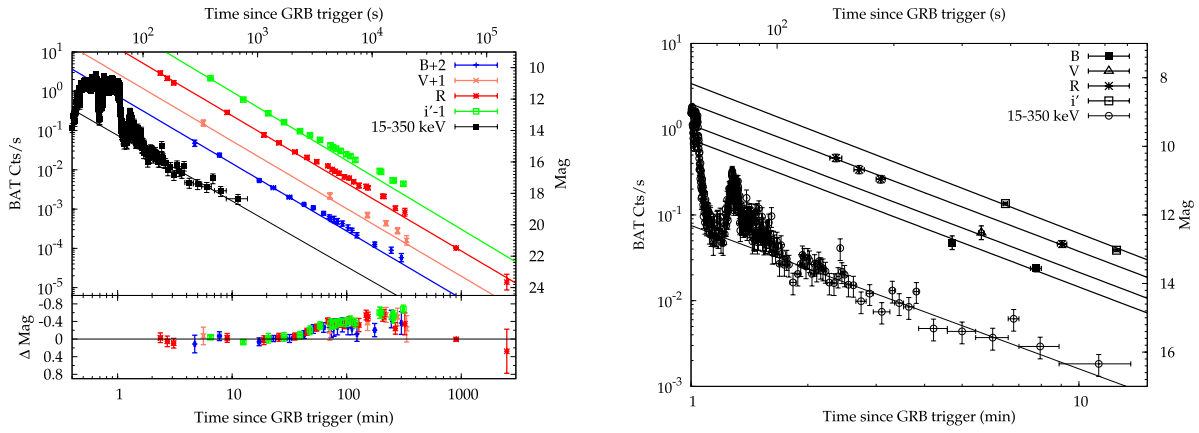


Fig. 1.— **Left:** FTS BVR*i'* optical and *Swift*  $\gamma$ -ray light curves of GRB 061007. Optical light curves are fitted with a single power-law fits for  $t < 40$  min and the background-subtracted  $\gamma$ -ray light curve is fitted with a similar power law to data at  $t > 120$  s. The BAT count rate (counts per sec per fully illuminated detector for an equivalent on-axis source) and optical magnitudes are given on the left and right vertical axes respectively. The lower panel shows the optical residuals after removal of the corresponding power law (see Table 2), highlighting the presence of a broad bump in all filters for  $t > 40$  min. Late time R-band photometry from VLT and Magellan images are included at  $t \sim 1000$  and  $t \sim 2500$  min respectively and are consistent with extrapolation of the power-law decay. **Right:** An expanded view of the optical and  $\gamma$ -ray light curves at early time ( $1 < t < 11$  min).

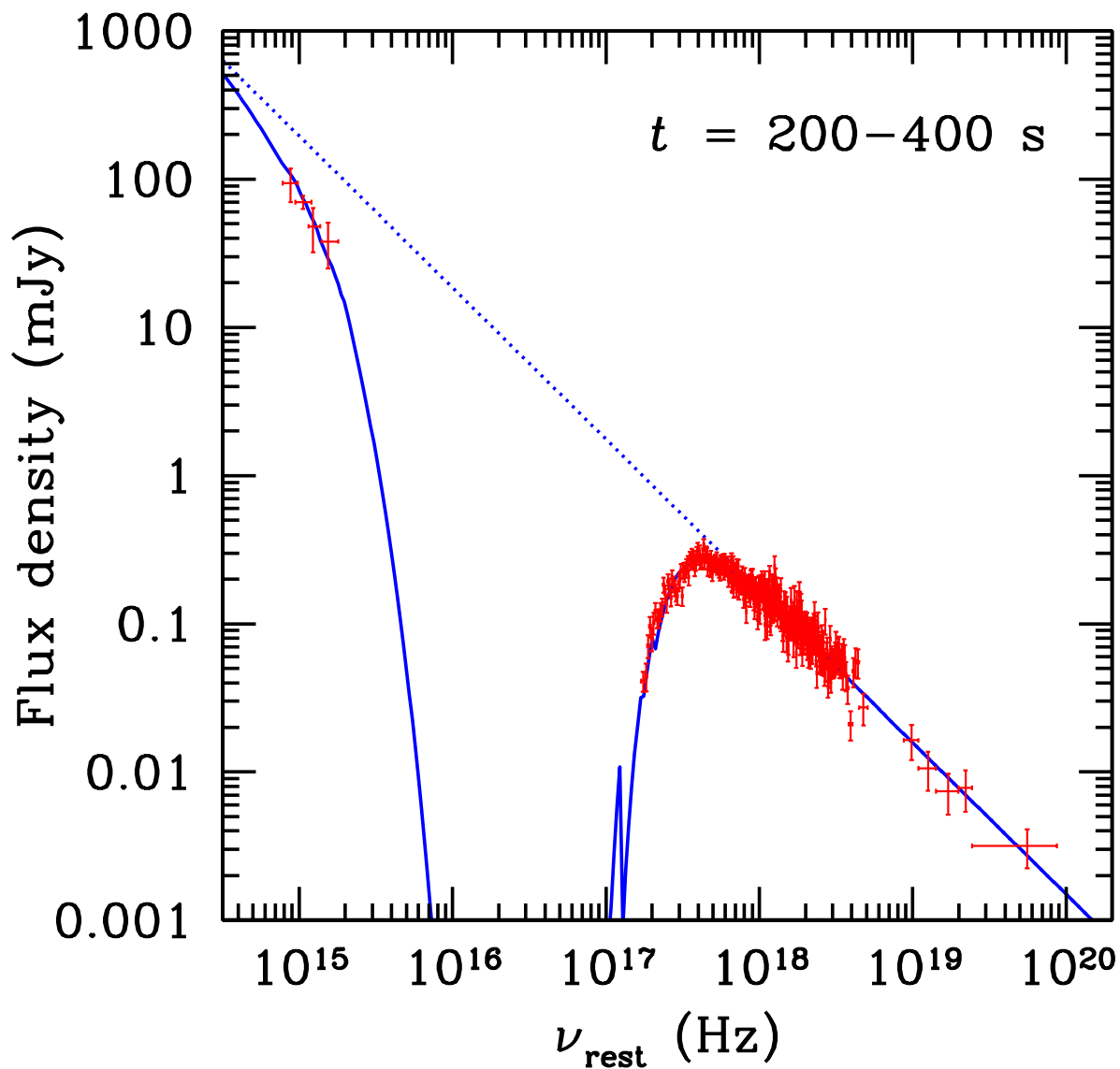


Fig. 2.— Broad-band optical to  $\gamma$ -ray spectral energy distribution derived for the time interval  $200 < t_{\text{obs}} < 400$  s, fitted with an absorbed power law with  $\beta(\text{opt-X-}\gamma) = 1.02 \pm 0.05$  and rest frame extinction  $A_V(\text{SMC}) = 0.48 \pm 0.19$  mag (solid line). The unabsorbed power law is also shown (dotted line).

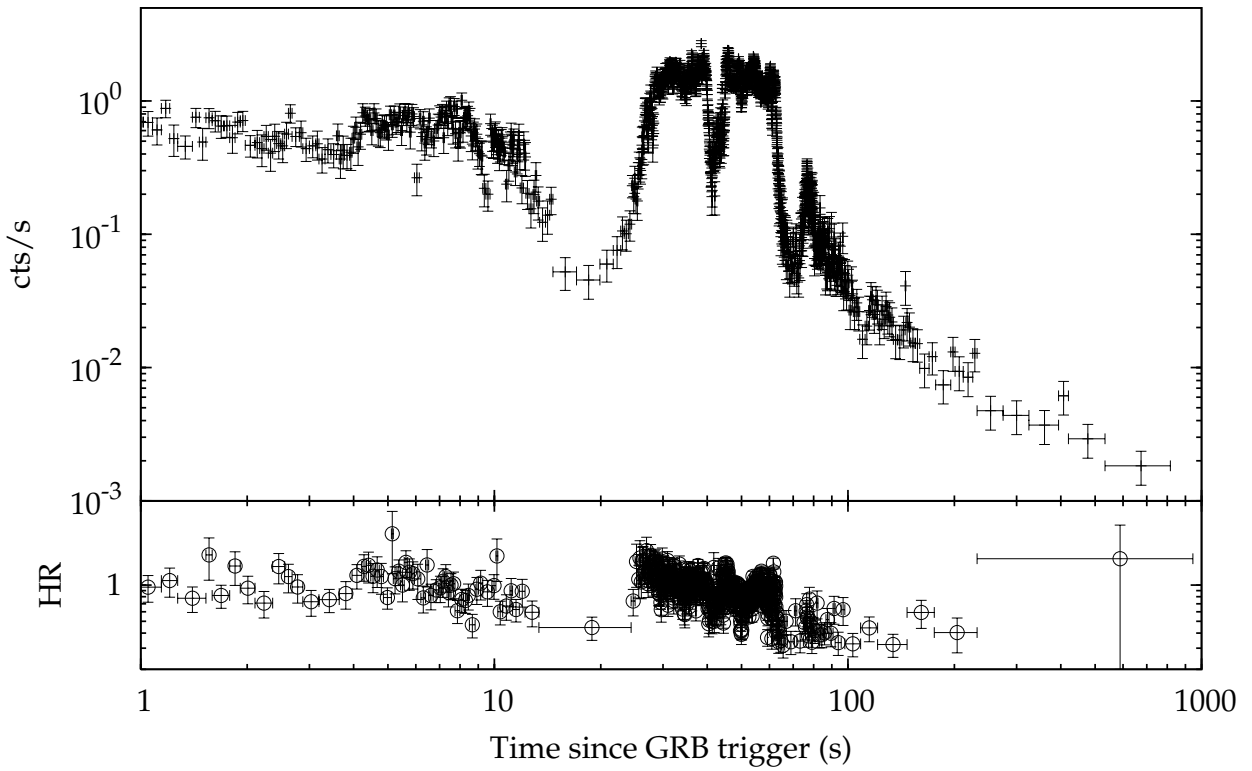


Fig. 3.— Evolution of the hardness ratio (HR), derived from comparison of count rates in 50–350 and 15–50 keV bands, compared with the BAT (15–350 keV), showing a marginal softening of the  $\gamma$ -ray spectrum with time.